Received: 8 May 2023 | Revised: 23 January 2024 | Accepted: 23 January 2024

DOI: 10.1002/mrm.30046

RESEARCH ARTICLE

Magnetic Resonance in Medicine

Robust EMI elimination for RF shielding-free MRI through deep learning direct MR signal prediction

Yujiao Zhao[1,2] | **Linfang Xiao**[1,2] | **Jiahao Hu**[1,2] | **Ed X. Wu**[1,2]

[1]Laboratory of Biomedical Imaging and Signal Processing, The University of Hong Kong, Hong Kong, People's Republic of China

[2]Department of Electrical and Electronic Engineering, The University of Hong Kong, Hong Kong, People's Republic of China

Correspondence
Ed X. Wu, Department of Electrical and Electronic Engineering, The University of Hong Kong, Hong Kong SAR, China
Email: ewu@eee.hku.hk

Funding information
Hong Kong Research Grant Council, Grant/Award Numbers: HKU17104020, HKU17112120, HKU17127021, HKU17127022, HKU17127121, HKU17127523, HKU17127723, R7003-19F

Abstract

Purpose: To develop a new electromagnetic interference (EMI) elimination strategy for RF shielding-free MRI via active EMI sensing and deep learning direct MR signal prediction (Deep-DSP).

Methods: Deep-DSP is proposed to directly predict EMI-free MR signals. During scanning, MRI receive coil and EMI sensing coils simultaneously sample data within two windows (i.e., for MR data and EMI characterization data acquisition, respectively). Afterward, a residual U-Net model is trained using synthetic MRI receive coil data and EMI sensing coil data acquired during EMI signal characterization window, to predict EMI-free MR signals from signals acquired by MRI receive and EMI sensing coils. The trained model is then used to directly predict EMI-free MR signals from data acquired by MRI receive and sensing coils during the MR signal-acquisition window. This strategy was evaluated on an ultralow-field 0.055T brain MRI scanner without any RF shielding and a 1.5T whole-body scanner with incomplete RF shielding.

Results: Deep-DSP accurately predicted EMI-free MR signals in presence of strong EMI. It outperformed recently developed EDITER and convolutional neural network methods, yielding better EMI elimination and enabling use of few EMI sensing coils. Furthermore, it could work well without dedicated EMI characterization data.

Conclusion: Deep-DSP presents an effective EMI elimination strategy that outperforms existing methods, advancing toward truly portable and patient-friendly MRI. It exploits electromagnetic coupling between MRI receive and EMI sensing coils as well as typical MR signal characteristics. Despite its deep learning nature, Deep-DSP framework is computationally simple and efficient.

KEYWORDS

deep learning, electromagnetic interference, EMI, portable MRI, RF shielding, ultralow field

1 | INTRODUCTION

MRI is a versatile imaging modality that provides noninvasive, nonionizing, and quantitative characterization of biological tissues. After five decades of development, it is now a routine procedure for clinical diagnoses and preclinical investigations, making a tremendous impact in modern health care.[1–3] On the other hand, the accessibility of MRI is low, and its distribution is extremely inhomogeneous worldwide,[4] primarily due to the cost-prohibitive nature and special infrastructural requirements associated with existing high-field (1.5 T or 3 T) superconducting MRI scanners. Consequently, there has been a growing interest and urgency to address the unmet clinical needs and global health-care disparities by developing ultralow-field (ULF) MRI scanners that operate below 0.1 T for low-cost and/or portable imaging applications.[5–14] Recent ULF MRI technology developments in both system engineering[15–19] and computing[20–23] have yielded promising results and have led to diagnostically useful information especially in intensive care.[19,24–27]

MR signals are susceptible to electromagnetic interference (EMI) signals at frequencies close to Larmor frequency. Clinical high-field MRI prevents EMI signals using bulky and fully enclosed RF shielding room and high-quality electronics (e.g., MRI scanner electronics or MRI compatible medical devices/equipment with minimal EMI emission) inside the shielding room. However, this passive solution in turn comes with hardware costs and stringent installation requirements, which pose a major barrier to the accessibility, portability, and patient-friendliness of both ULF and high-field MRI scanners.

An active EMI elimination approach presents an alternative solution to remove EMI signals through active and simultaneous EMI sensing via multiple EMI sensing coils during scanning, and retrospective prediction and cancelation of EMI signals detected by MRI receive coil.[28–35] From an RF signal propagation point of view, relationships among EMI signals detected by various coils that are positioned and/or oriented differently can be well characterized by the electromagnetic coupling among coils. Such relationships allow EMI signals detected by the MRI receive coil to be predicted from EMI signals simultaneously acquired by one or multiple EMI sensing coils, thus enabling retrospective EMI cancelation through postprocessing. Specifically, an analytical formulation was developed to predict EMI signals detected by the MRI receive coil using frequency domain transfer functions between the MRI receive coil and EMI sensing coils.[28] Several methods based on this concept have been subsequently introduced and demonstrated for ULF MRI scanners.[29–33] One example is EDITER,[31] which extends the frequency domain transfer function method for time domain implementation, yielding improved performance by accommodating dynamically varying EMI sources.

In our recent work, a deep learning–based approach was developed to model and predict EMI signals from the acquired MRI receive coil signals.[19,34,35] In contrast to the analytical methods mentioned previously, this method assumes that the relationship between EMI signals detected by EMI sensing coils and MRI receive coil, although linear in theory, can be better approximated in practice through a versatile time domain convolution neural network (CNN) model that incorporates nonlinear operations. This assumption has been well supported by successful shielding-free 0.055T brain imaging of a cohort of about 100 healthy volunteers and patients in our laboratory,[19,34,35] leading to improved performance over the EDITER method. Additionally, this method has also been demonstrated for a much higher frequency regime on a 1.5T MRI scanner with incomplete RF shielding.[34,35]

Despite the success in predicting and retrospectively reducing EMI signals so far, the aforementioned methods[19,29–35] are certainly inadequate to enable truly RF shielding-free MRI. In practice, EMI nature and behaviors can be extremely complex. For example, in realistic and diverse unshielded imaging situations, EMI signals can be emitted from multiple sources. They can be strong and vary temporally and/or spatially. During scanning, surrounding environments can also change, such as due to subject position changes or movements of nearby attending staff and equipment. Note that transfer functions depend on relative location geometries of EMI sensing coils with respect to MRI receive coil, EMI sources, and surrounding environments. Therefore, the changes in EMI sources or/and surrounding environments can alter the actual transfer functions between the MRI receive coil and EMI sensing coils. These real-world scenarios can easily compromise the performance of these existing EMI-elimination methods. For RF shielding-free MRI to become a reality for robust portable or point-of-care applications, it is imperative to develop more effective strategies.

In this study, we develop a new EMI elimination strategy for RF shielding-free MRI, termed deep learning–based direct MR signal prediction (Deep-DSP). Specifically, a time-domain residual U-Net model is trained after scanning to directly predict EMI-free MR signals from the signals detected by MRI receive coil and EMI sensing coils. For training, the data for MRI receive coil were synthesized from the EMI data and a set of arbitrary EMI-free MR signals. We demonstrate that this strategy works effectively in the presence of strong EMI for both 0.055T and 1.5T MRI, yielding significantly improved image quality over the existing methods. The proposed

method also works robustly with few EMI sensing coils or without dedicated EMI characterization data.

2 | METHODS

2.1 | Existing active EMI sensing and elimination methods

All active EMI sensing and elimination methods so far[19,28–35] use one or multiple EMI sensing coils. During scanning, they simultaneously detect EMI signals only, whereas the MRI receive coil detects both frequency-encoding (FE) MR signals and EMI signals.

Analytical transfer function–based EMI elimination methods estimate electromagnetic coupling functions among coils and then use them to retrospectively predict and remove EMI signal components from MRI receive-coil signals.[28–30] In practice, these transfer functions can be obtained numerically by linearly fitting the spectra of EMI signals from all EMI sensing coils to that of MRI receive-coil signal among all EMI characterization data. EMI characterization data can be acquired when no MR signal components are present (e.g., through separate scans without RF excitation or sampling within a period when MR signals are expected to be negligible).

The EDITER method extends this analytical frequency-domain transfer function concept to time domain.[31] Assuming that frequency-domain transfer functions are relatively compact, EDITER implements EMI prediction in time domain as linear convolutions using finite and small convolution kernels. It accommodates dynamically changing EMI sources by dividing the acquired data into sub–data sets through empirical thresholding with respect to the transfer function characteristics, and works without separate or dedicated EMI characterization data.

In parallel, the recent deep learning approach relates EMI signals detected by all EMI sensing coils to EMI signals detected by MRI receive coils through a time-domain five-layer CNN model.[19,34,35] Such a CNN model consists of a combination of multiple layers of simple operations (such as linear convolution and nonlinear activation) that are trained in a data-driven manner, leading to improved EMI elimination.[34]

2.2 | Proposed Deep-DSP

The proposed Deep-DSP is designed to directly predict EMI-free MR signals (instead of EMI signals in all other existing methods) from signals acquired by the MRI receive coil and EMI sensing coils. The overall framework is illustrated in Figure 1. As in all other active EMI cancelation methods, one or multiple EMI sensing coils are used in Deep-DSP (Figure 1A). They are placed around and within the scanner to actively detect radiative EMI signals from both external environments and internal electronics while receiving no MR signals.

Within each TR during scanning, the MRI receive coil samples data within the MR signal acquisition and EMI signal characterization windows, with acquired data denoted as $r_0(t)$ and $r_0^{\text{char}}(t)$, respectively (Figure 1B). Note that the MRI receive-coil signal $r_0^{\text{char}}(t)$ contains no or negligible MR signal component due to absence of any RF excitation within the second window (i.e., EMI signal characterization window). Meanwhile, within two windows, each EMI sensing coil also samples EMI-only data, which are denoted by $s_k(t)$ and $s_k^{\text{char}}(t)$ $(k = 1, 2, \ldots, N_s)$, respectively. N_s denotes the number of EMI sensing coils.

The Deep-DSP model is trained by both synthetic and experimental data. Specifically, after scanning, one-dimensional (1D) temporal EMI-free MR signals $x_{\text{GT}}(t)$ from one arbitrary MR k-space data set (e.g., one typical simulated or experimental data set) are added into experimental EMI-only MRI receive-coil signals $r_0^{\text{char}}(t)$ to first synthesize EMI-contaminated MRI receive-coil signals $r_0^{\text{syn}}(t)$ (see green box in Figure 1C). A residual U-Net model is then trained with synthetic $r_0^{\text{syn}}(t)$ and experimental $s_k^{\text{char}}(t)$ $(k = 1, 2, \ldots, N_s)$ being used as model inputs, while the corresponding ground-truth $x_{GT}(t)$ is the model target.

The trained model is then applied to predict EMI-free MR signal component $x_0(t)$ from experimental signals $r_0(t)$ and $s_k(t)$ $(k = 1, 2, \ldots, N_s)$ collected within the MR signal-acquisition window (Figure 1D). This MR signal-prediction procedure is repeated for every individual FE line, creating EMI-free k-space data before any averaging or/and image reconstruction.

2.3 | Deep-DSP model architecture, implementation, and training

Early studies have demonstrated that U-Net can facilitate information propagation,[36] whereas ResNet enables the increase of model capacity.[37] As such, this study adopted a residual U-Net architecture.[38] The residual U-Net model, being deeper and more versatile than the simple CNN model, is used to further improve the characterization of the EMI signal relationship among coils, especially when EMI characteristics and/or environments become complex. Additionally, during training, the model captures the characteristic difference between EMI signals and MR k-space signals, which serves as prior knowledge for accurate MR signal prediction. Specifically, the model

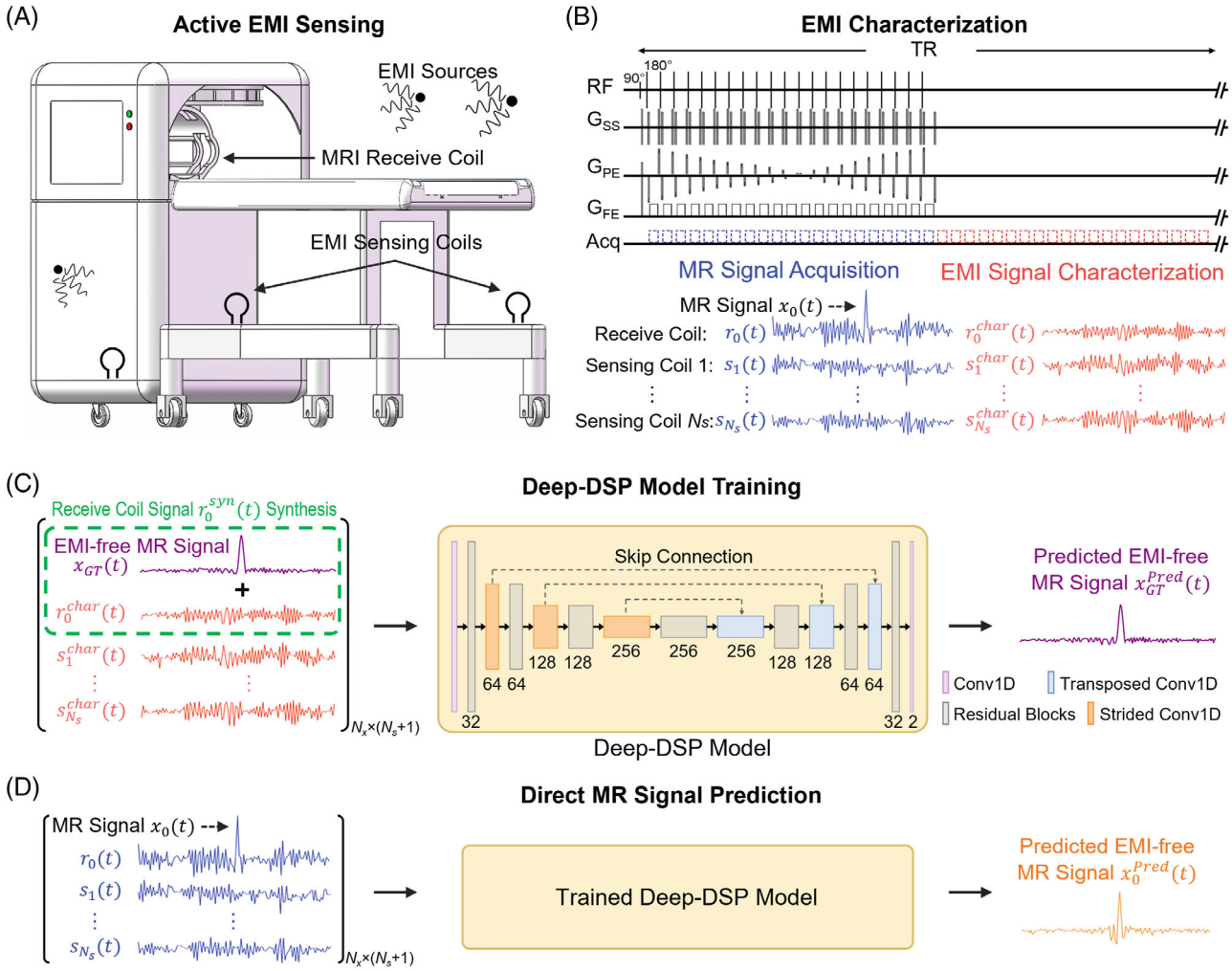

FIGURE 1 The proposed deep learning direct MR signal prediction (Deep-DSP) framework and its implementation on a low-cost, shielding-free 0.055T brain MRI scanner. (A) Multiple electromagnetic interference (EMI) sensing coils are installed to actively detect EMI signals during scanning. (B) Illustration of 3D fast spin-echo acquisition windows for MR signal acquisition and EMI signal characterization. Within each TR, data sampled by MRI receive coil during two windows are denoted as $r_0(T)$ and $r_0^{\text{char}}(t)$, respectively. Meanwhile, data sampled by each EMI sensing coil during the two windows are denoted as $s_k(t)$ and $s_k^{\text{char}}(t)$ ($k = 1, 2, \ldots, N_s$), respectively. (C) A residual U-Net model is trained using signals detected during the EMI signal characterization window. EMI-free MR signals $x_{GT}(t)$ from an arbitrarily chosen MR data set are first added to EMI-only MRI receive coil signals $r_0^{\text{char}}(t)$ to synthesize EMI-contaminated MRI receive coil signals $r_0^{\text{syn}}(t)$. For model training, synthetic EMI-contaminated MR signals and experimental EMI sensing coil signals $s_k^{\text{char}}(t)$ ($k = 1, 2, \ldots, N_s$) are used as model inputs, whereas EMI-free MR signals $x_{\text{GT}}(t)$ serve as model target or output. (D) Trained model is then used to predict MR signals from MRI receive-coil signals $r_0(t)$ and EMI sensing-coil signals $s_k(t)$ ($k = 1, 2, \ldots, N_s$). Note that the EMI signal characterization window is not an absolute requirement. In practice, outer k-space of data acquired within the MRI signal acquisition window can serve as alternative EMI characterization data for model training.

was implemented using a 4-scale U-Net. Each scale had an identity skip connection between strided convolution downscaling and transposed convolution upscaling, both of which were applied with a kernel size of 2. The number of channels in each layer from the first to the fourth scale was 32, 64, 128 and 256, respectively. Four successive residual blocks were used in the downscaling and upscaling of each scale. Model input was a 2D matrix with a size of $N_x \times 2(1 + N_s)$, where N_x is the number of points in one FE line, while $2(1 + N_s)$ is the number of channels corresponding to real and imaginary parts of 1D temporal signals from one MRI receive coil and N_s EMI sensing coils. Model output was a 2D matrix with a size of $N_x \times 2$.

In this study, one experimental axial 3D T_2-weighted (T_{2W}) brain MR k-space data set acquired from a standard clinical 3T MRI scanner was arbitrarily chosen and treated as EMI-free MR signals. They were used to synthesize EMI-contaminated MRI receive coil signals for

Deep-DSP model training. Specifically, this T_{2W} brain data set was acquired on a 3T Philips scanner (Achieva; Philips Medical Systems, Best, The Netherlands) using a single-channel head coil and 3D fast spin echo (FSE) with TR/TE = 2500/213 ms, matrix size = 240 × 240 × 60, and isotropic resolution = 1 mm. Raw k-space data were truncated along the FE direction to a size of $N_x \times 240 \times 60$ and then transformed to image space. After normalizing the image intensity to approximately match those observed from MRI receive-coil signals (in absence of EMI signals), the data were then transformed back to k-space. Individual EMI-free FE lines (a total of 14400) were extracted in a pseudo-random order and added to the MRI receive-coil signals acquired within the EMI signal characterization window after scanning to synthesize $r_0^{syn}(t)$.

To eliminate EMI in each data set, a model was trained by minimizing L1 loss using the Adam optimizer[39] with batch size = 64, initial learning rate = 0.0002, $\beta_1 = 0.9$, and $\beta_2 = 0.999$ for 40 epochs. Without optimization, the typical training time for each model was about 6 min on a Quadro RTX 8000 GPU and Intel Core i9-10 900X CPU using *PyTorch* 1.8.1 package on Ubuntu 18.04.5 LTS (Linux 5.4.0-77-generic).

2.4 | Performance evaluation

Deep-DSP was evaluated on a home-built shielding-free 0.055T brain MRI scanner that was recently developed in our laboratory.[19] Using a permanent Samarium-cobalt magnet, it operates using a standard AC power outlet and is low cost to build. Ten EMI sensing coils (same coils as in our recent studies[19,34]) were placed around the scanner and inside the electronic cabinet to detect EMI signals from both the external environment and internal scanner electronics during scanning. Specifically, three were placed in the vicinity of the patient head holder, two on each side (left and right) underneath the patient bed, and two in the vicinity of gradient and RF amplifiers inside the electronic cabinet, and one underneath the scanner.

2.4.1 | Evaluation by simulations

The effectiveness of Deep-DSP was first examined using simulated data sets. EMI-free brain and phantom data sets acquired on the 3T Philips scanner were used as ground truth. EMI-contaminated data sets were obtained by adding experimental EMI data acquired on the shielding-free 0.055T MRI scanner[19] with RF transmitter power off (i.e., in absence of any MR signal) to the ground truth EMI-free data sets. To assess the EMI elimination performance, the SNR of ground-truth and EMI-eliminated images were calculated, and the difference or error maps between ground-truth and EMI-eliminated images were computed and quantified by normalized RMS errors (NRMSEs).

2.4.2 | Experimental evaluation by human brain imaging on a shielding-free 0.055T MRI scanner

The Deep-DSP model was evaluated with shielding-free 0.055T brain data sets. Three imaging protocols were implemented. They were 3D T_{2W} FSE (TR/TE = 1500/202 ms, echo train length [ETL] = 21, bandwidth [BW] = 10 kHz, FOV = 250 × 250 × 320 mm^3, acquisition matrix = 128 × 126 × 32, and number of excitations [NEX] = 2), 3D fluid-attenuated inversion recovery [FLAIR]–like FSE (TR/TE = 500/129 ms, ETL = 13, BW = 10 kHz, FOV = 250 × 250 × 320 mm^3, acquisition matrix = 128 × 117 × 32, and NEX = 4), and 3D T_1-weighted (T_{1W}) gradient-recalled echo (TR/TE = 52/13 ms, flip angle = 40°, BW = 6.25 kHz, FOV = 250 × 250 × 320 mm^3, acquisition matrix = 128 × 128 × 32, and NEX = 2). All experiments involving human subjects were approved by the local institutional review board, and written consents were obtained.

2.4.3 | Experimental evaluation by phantom imaging on a 1.5T MRI scanner with incomplete RF shielding

The potential applicability of Deep-DSP to high-field MRI was also examined. Specifically, one phantom data set was acquired on a whole-body 1.5T clinical MRI scanner with the RF shielding room door open. A head coil with eight channels was used as the MRI receive coils, whereas a separate knee coil with eight channels was placed on the patient bed, serving as EMI sensing coils. A 2D gradient-recalled echo protocol was used with TR/TE = 420/9 ms, BW = 25 kHz, and acquisition matrix = 200 × 200 × 20.

For comparison, the EMI elimination was also performed using EDITER[31] and our recently developed CNN method.[19] EDITER was implemented with the publicly available codes,[31] and its kernel size and threshold value were optimized to ensure the best performance as in our recent study.[34] Furthermore, the effect of the reduced number of EMI sensing coils on the performance of the proposed Deep-DSP and existing EDITER and CNN methods was examined. Their performance in absence of dedicated EMI characterization data (i.e., acquired within EMI signal-characterization window shown in Figure 1B) was

also examined. In this case, data acquired by MRI receive and EMI sensing coils within the MR signal acquisition window were chosen to serve as the EMI characterization data. To avoid the potentially strong MR signals at k-space center, only the outer 50% of the k-space data were used for this EMI characterization purpose.

3 | RESULTS

Figure 2 presents the typical EMI elimination results from a simulated brain data set. EDITER and CNN methods estimated EMI signals and subtracted them from the MRI receive coil signals, whereas Deep-DSP directly predicted MR signals. Before EMI elimination, brain images were mostly immersed within EMI noise. Deep-DSP accurately predicted MR signals, effectively eliminating the strong EMI artifacts as indicated by the error maps. Moreover, it yielded approximately 42% and 33% more NRMSE reduction compared with the EDITER and CNN methods, respectively. Figure S1 presents the influence of training data size on three EMI elimination methods when performing EMI elimination in Figure 2. With a small training data size (2-k FE lines), all three methods exhibited slightly degraded EMI elimination performance. Meanwhile, Deep-DSP still led to the smallest NRMSE. With relatively larger training data size (8 k or 4 k), the degradation was negligible for all three methods. These results indicated that the superior Deep-DSP performance did not critically rely on a large training data size.

For the simulated brain data set with reduced EMI signal level, Figure S2 shows the results from all three methods. Both EDITER and CNN results were largely improved when compared to those with strong EMI

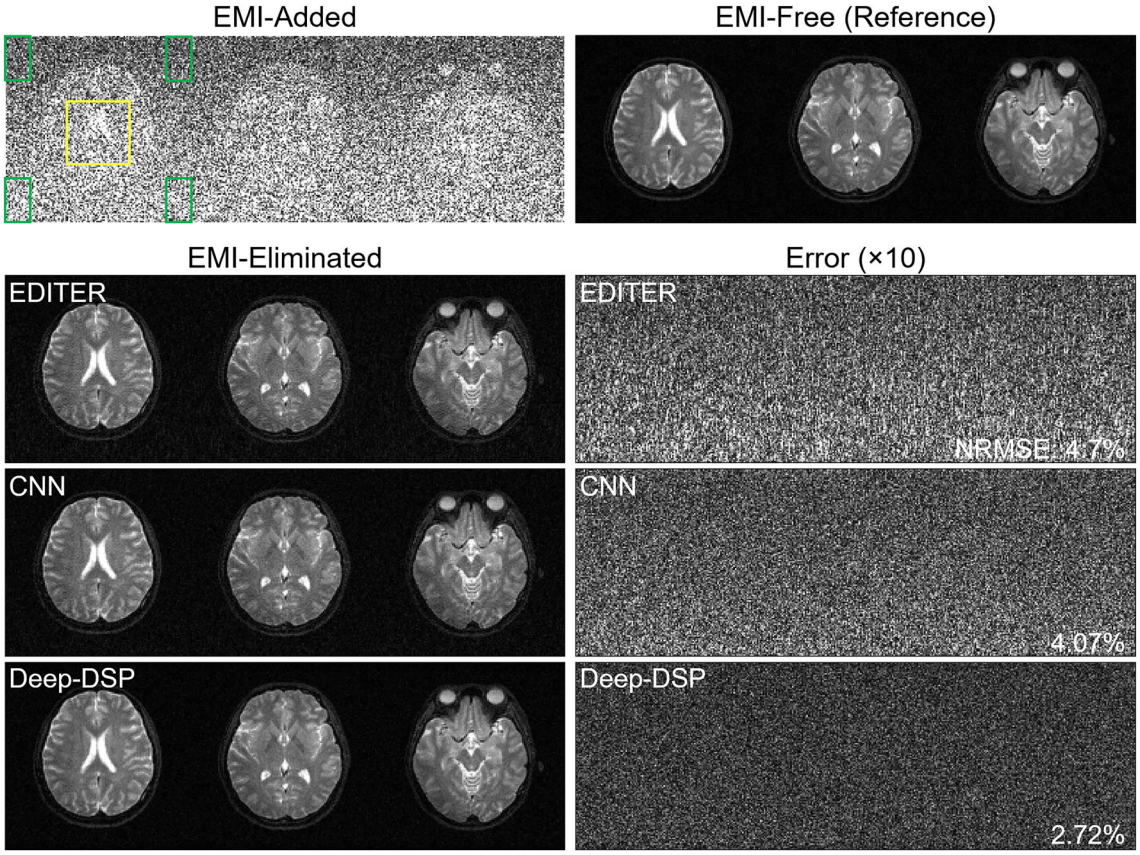

FIGURE 2 Electromagnetic interference (EMI) elimination for simulated brain data set. The T_2-weighted (T_{2W}) brain data set acquired at 3 T was used as ground truth. One EMI data set acquired at 0.055 T with RF transmitter power off (i.e., no MR signal) was retrospectively added into the ground truth to form EMI-contaminated data sets. EMI elimination was performed using EDITER, the deep learning convolutional neural network (CNN) method, and the proposed deep learning direct MR signal prediction (Deep-DSP) method. Images without and with EMI elimination are displayed using the same scaling. Deep-DSP accurately predicted EMI-free MR signals from EMI-added MRI receive coil signals and EMI sensing coil signals, with neither EMI artifacts nor pseudo-structures being observed in error maps (i.e., differences between EMI-free reference and EMI-eliminated images). Normalized RMS error (NRMSE) and SNR quantification (Table S1) further demonstrated the significantly improved EMI elimination performance of Deep-DSP over existing EDITER and CNN methods. The yellow and green boxes indicate signal and noise regions of interest for SNR calculation, respectively.

signals in Figure 2. This likely occurred because when the EMI signal level was relatively low, the inaccurate EMI signal relationship estimation in EDITER and CNN due to coil baseline electronic noise and its propagation/amplification were alleviated, thus leading to reduced EMI signal prediction errors. Nevertheless, Deep-DSP still achieved more effective EMI elimination than the EDITER and CNN methods. The residual error histograms computed from error maps are shown in Figure S3, further illustrating the improvement of Deep-DSP over the two existing methods in terms of reduced error bias and its SD. Note that the reduced-error SD further improved the resulting image SNR, as supported by Table S1.

Figure 3 shows the results of applying EMI elimination without dedicated EMI characterization data (i.e., using part of the k-space data acquired within the MR signal acquisition window instead) to the simulated brain data set in Figure 2. This evaluation is relevant to certain imaging protocols in which, for example, EMI characterization data are unavailable due to the need to preserve the shortest possible TR for imaging flexibility. Note that outer peripheral k-space data (50% of total) were used here as EMI characterization data. For all three methods, the EMI elimination results were comparable to those using dedicated EMI characterization data in Figure 2. These simulation results indicated that Deep-DSP outperformed existing EMI prediction/cancelation methods even in absence of separate or dedicated EMI characterization data.

Figure 4 compares the Deep-DSP with EDITER and CNN methods for experimental shielding-free 0.055T human brain imaging in the presence of strong broadband and narrowband EMI from external environments. Results at three slice locations are shown. Consistent with simulation results, Deep-DSP achieved significant image-quality improvement. Note that, when EMI signals were extremely strong, distinct EMI artifacts were still present in EDITER results, but largely absent in CNN and Deep-DSP results. In general, Deep-DSP produced more effective EMI elimination than EDITER and CNN, as supported by SNR quantification in Table S2.

Using the raw data set in Figures 4–6 demonstrates the effect of using different numbers of EMI sensing coils ($N_s = 1$, 2, 4, and 10) or no dedicated EMI characterization data on EMI elimination performance. Overall, Deep-DSP yielded the best results, as evident from the image results shown in Figures 5 and 6 and spectral analysis results in Figure S4. With fewer EMI sensing coils ($N_s = 1$ or 2), the degradation of EDITER performance became pronounced, leading to a higher level of EMI residual artifacts compared with the results using 4 or 10 EMI sensing coils. Such degradation was largely expected, because the analytical EDITER approach prefers the number of EMI sensing coils to be larger than or equal to the number of EMI sources for accurate EMI signal estimation. Meanwhile, the deep learning–based CNN and Deep-DSP methods exhibited better tolerance. Note that Deep-DSP

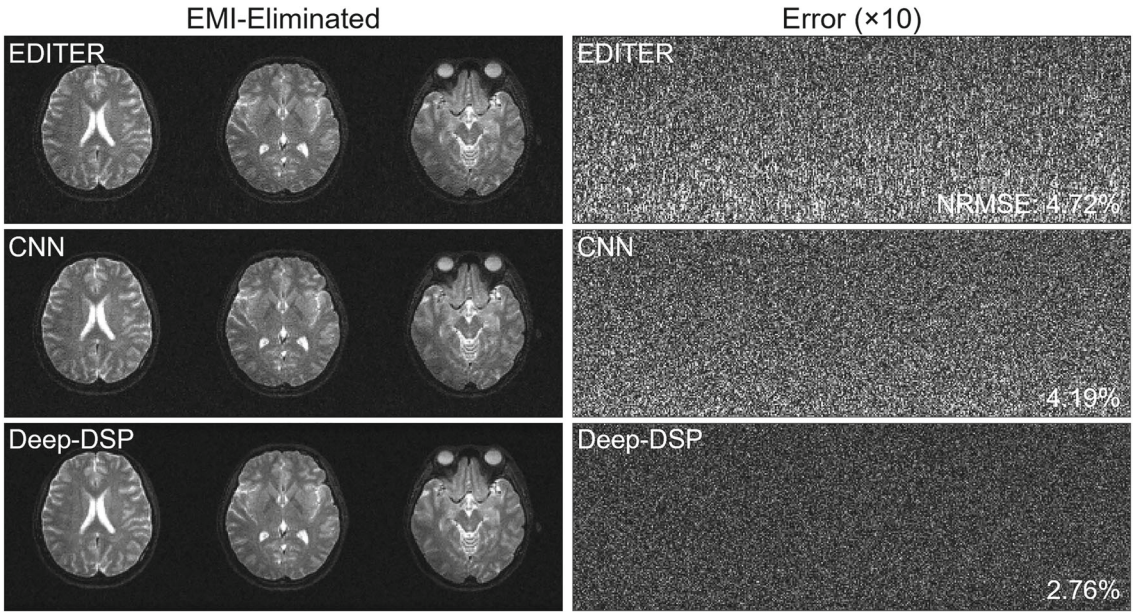

FIGURE 3 Electromagnetic interference (EMI) elimination for simulated brain data set without separate or dedicated EMI characterization data. The T_2-weighted brain data set and EMI data set were the same as those used for Figure 2. Outer 50% k-space data acquired by MRI receive coil and EMI sensing coils within MR signal acquisition window was used for numerical fitting by EDITER and model training by convolutional neural network (CNN) or deep learning convolutional neural network (Deep-DSP). Deep-DSP still achieved more effective EMI elimination compared with EDITER and CNN. NRMSE, normalized RMS error.

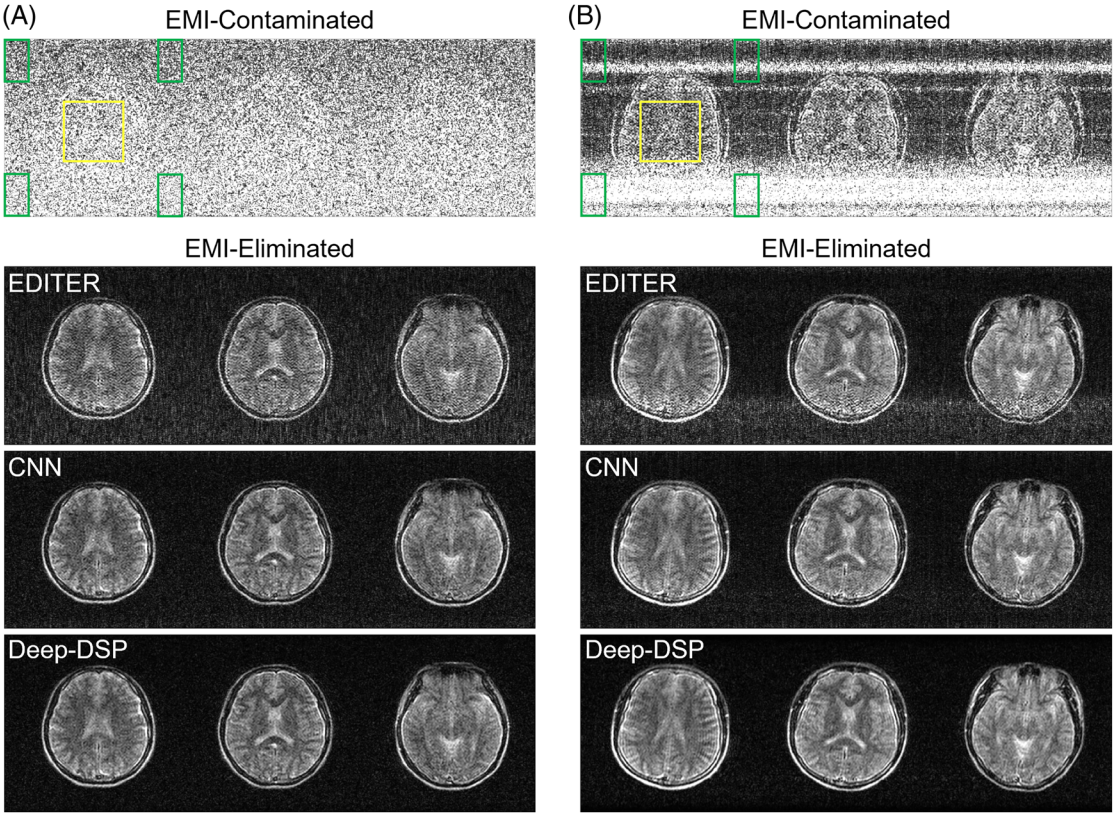

FIGURE 4 Electromagnetic interference (EMI) elimination for experimental shielding-free 0.055T brain imaging in the presence of strong broadband (A) and narrowband (B) EMI. The T_2-weighted brain data sets were acquired from 2 healthy adult subjects using the 3D fast spin-echo protocol. EMI elimination was performed using EDITER, convolutional neural network (CNN), and deep learning convolutional neural network (Deep-DSP). Images at three slice locations contaminated by broadband or narrowband EMI, without and with EMI elimination, are displayed using the same scaling. Note that the display of the strong narrowband EMI was saturated. The yellow and green boxes indicate regions of interest for SNR quantification in Table S2. Before EMI elimination, images were severely corrupted by EMI artifacts. Deep-DSP accurately predicted MR signals, leading to significantly improved image quality.

still produced reasonable EMI elimination with only one EMI sensing coil in this case. Furthermore, EMI elimination using 50% outer k-space data acquired within the MR signal-acquisition window produced results largely comparable to those using data acquired within the EMI signal-characterization window (Figure 6). These experimental results again demonstrated that Deep-DSP was effective and robust, even with few EMI sensing coils or/and without dedicated EMI characterization data.

Figure 7 shows the EMI elimination results of shielding-free 0.055T brain data sets in coronal T_1-weighted, T_{2W}, and FLAIR imaging. Note that, during training data preparation, only the axial T_{2W} brain data set was used to synthesize EMI-contaminated MRI receive-coil signals. Nevertheless, the trained models effectively predicted MR signals for these three coronal protocols. Together with the EMI elimination results in Figures S5–S7, these results indicated that trained Deep-DSP models were relatively insensitive to image contents/contrasts or field strengths.

The EMI elimination results of the 1.5T phantom data set with incomplete RF shielding are shown in Figure 8. Without EMI elimination, EMI artifacts severely compromised image quality. With EDITER and CNN using eight EMI sensing coils, EMI artifacts were reduced but still pronounced. With fewer EMI sensing coils, EMI artifacts in the EDITER and CNN results became more pronounced. In contrast, EMI artifacts were mostly eliminated in the Deep-DSP results even with few EMI sensing coils.

4 | DISCUSSION

In this study, we propose a novel active EMI elimination strategy to tackle the RF shielding-cage requirement for MRI. The proposed Deep-DSP directly predicts EMI-free MR signals from signals simultaneously acquired by MRI receive coil and EMI sensing coils. It exploits the electromagnetic coupling between MRI receive coil and EMI sensing coils as well as the typical MR signal

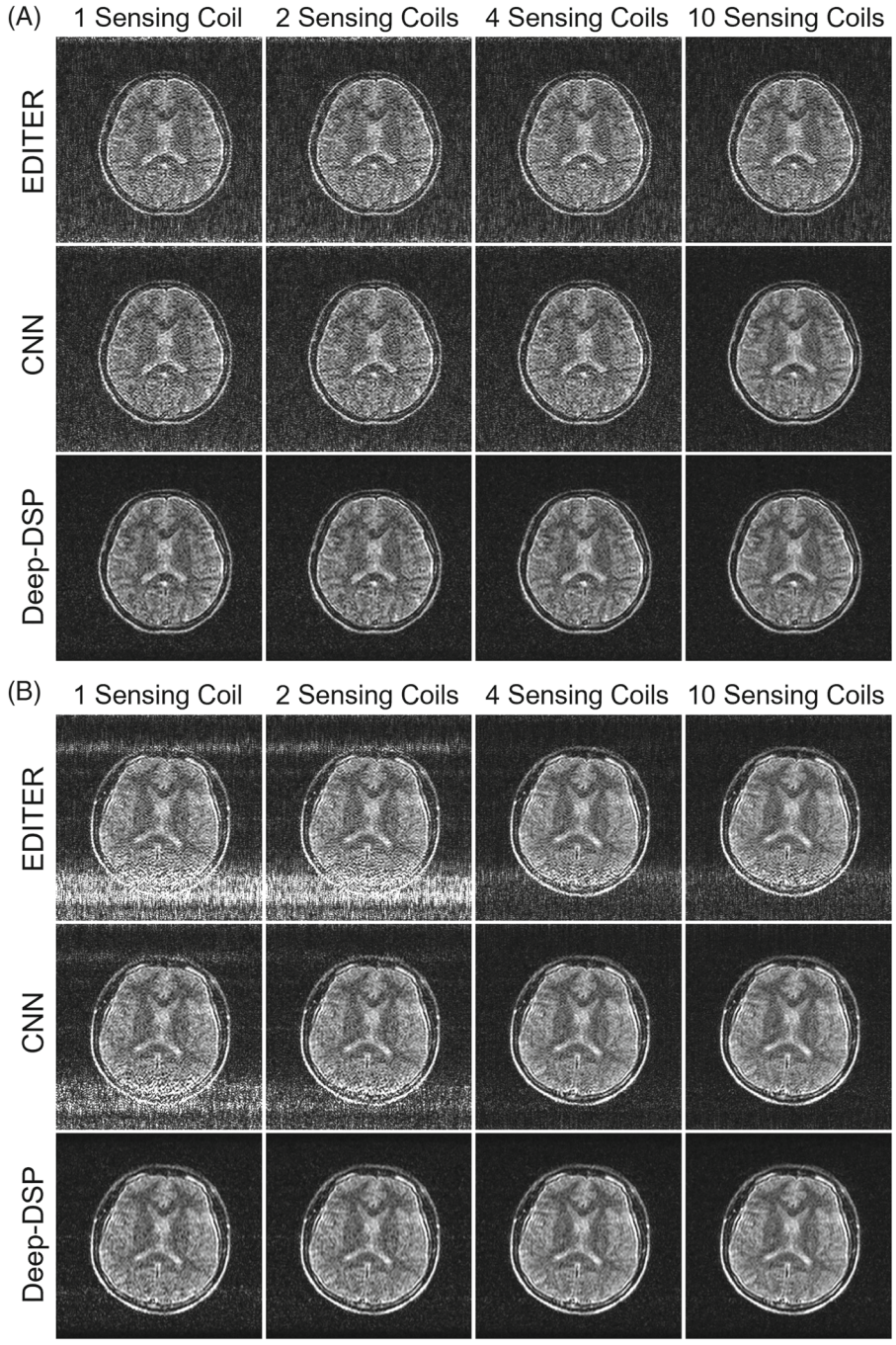

FIGURE 5 Electromagnetic interference (EMI) elimination results of experimental shielding-free 0.055T brain data sets in Figure 4 with different numbers of EMI sensing coils ($N_s = 1$, 2, 4, and 10). Raw T_2-weighted brain data sets were acquired in presence of strong broadband (A) and narrowband (B) EMI. The results demonstrated that deep learning convolutional neural network (Deep-DSP) outperformed EDITER and convolutional neural network (CNN), even with fewer EMI sensing coils.

characteristics in a data-driven manner through a time-domain residual U-Net model. We demonstrate that it works effectively, consistently outperforming the recently developed EDITER and CNN methods.

Effective EMI elimination is challenging in realistic unshielded imaging settings. First, EMI signals can be emitted by multiple and diverse sources (e.g., from external environments and internal low-cost scanner electronics). Analytical transfer function–based EMI elimination prefers the number of EMI sensing coils to be larger than or equal to the number of EMI sources for transfer function estimation using the numerical fitting procedure.[28] This suggests that effective and robust EMI elimination in practice requires multiple EMI sensing coils. Second, both MRI receive and sensing coils are unavoidably subject to baseline electronic noise that prevents accurate estimation of transfer functions in either frequency or time domain (e.g., through additive combination or even amplification). Third, EMI signal propagation chain inevitably can exhibit nonlinear responses.[40] Finally, EMI sources and/or surrounding environments often vary dynamically, altering the actual transfer functions during

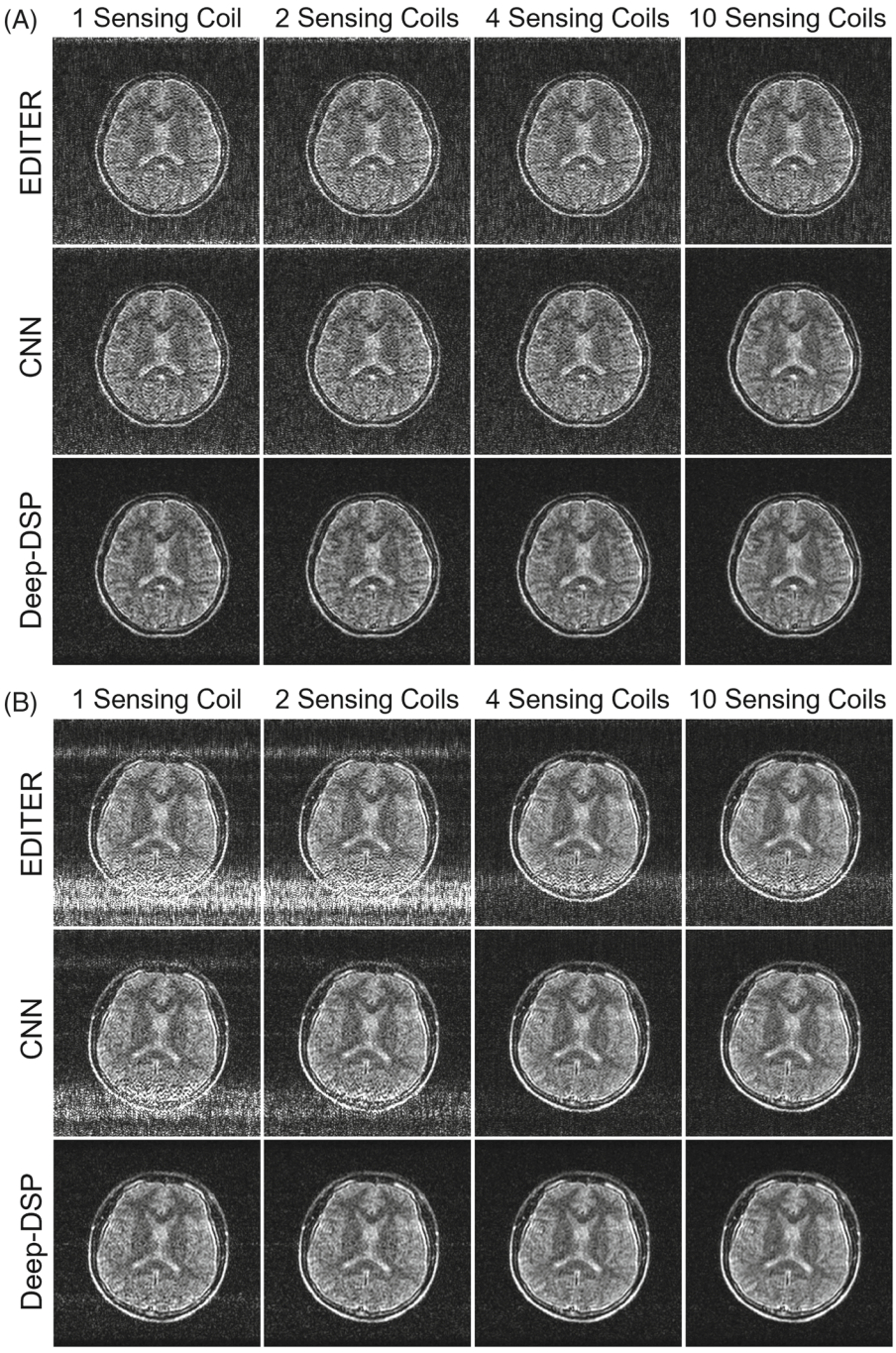

FIGURE 6 Electromagnetic interference (EMI) elimination results of experimental shielding-free 0.055T brain data sets in Figure 4 with different numbers of EMI sensing coils ($N_s = 1$, 2, 4, and 10) and without dedicated EMI characterization data. Raw T_2-weighted brain data sets were acquired in presence of strong broadband (A) and narrowband (B) EMI. The results demonstrated that deep learning convolutional neural network (Deep-DSP) outperformed EDITER and convolutional neural network (CNN), even with fewer EMI sensing coils and/or without separate EMI characterization data.

scanning when EMI characterization data are acquired. Altogether, these practical issues can easily compromise the performance of transfer function–based EMI elimination methods.[29–32] Unsurprisingly, a deep learning approach such as the CNN method produces improved EMI elimination by mitigating these complex and largely intractable issues in a data-driven and resilient manner.[34]

The proposed Deep-DSP approach is distinct from existing transfer function–based methods[29–33] as well as the deep learning–based CNN method.[19,34,35] Here, a neural network model is trained to directly predict EMI-free MR signals from signals acquired by MRI receive coil and EMI sensing coils. During training, the model learns EMI signal relationships among coils. In parallel, it also captures the characteristic difference between time-domain EMI signals and MR k-space signals, which serves as prior knowledge for accurate MR signal prediction (see Figure S8 for Deep-DSP EMI elimination using no EMI sensing coils). Note that, unlike all previous methods in which EMI signals are first predicted and then used to compute EMI-free MR signals through subtraction, Deep-DSP directly predicts EMI-free MR signals. It thus bypasses the baseline noise additive/amplification problem that is associated with the EMI signal-subtraction

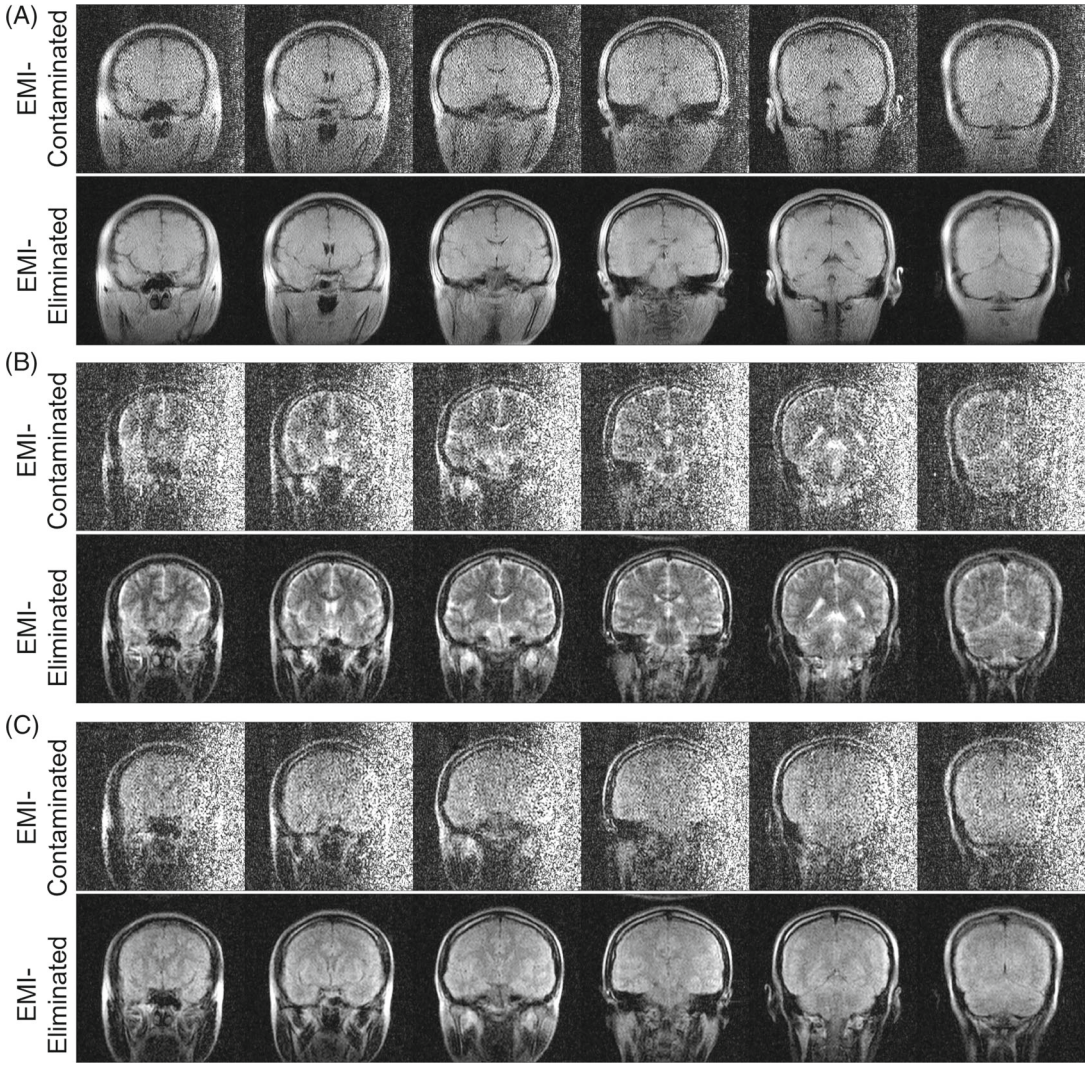

FIGURE 7 Application of the proposed deep learning convolutional neural network (Deep-DSP) to various imaging protocols on a shielding-free 0.055T brain MRI scanner. T_1-weighted (A), T_2-weighted (B), and fluid-attenuated inversion recovery (FLAIR)–like (C) coronal brain data sets were acquired from a healthy adult subject using 3D gradient-recalled echo, 3D fast spin echo (FSE), and short-TR 3D FSE, respectively. Electromagnetic interference (EMI)–free T_{2W} axial brain data were used to synthesize EMI-contaminated MRI receive coil signals for model training. Such trained models robustly predicted the T_{1W}, T_{2W}, and FLAIR-like coronal MR signals detected by the MRI receive coil, leading to effective elimination of EMI artifacts. The results illustrated that the trained models were not image content–specific nor contrast-specific.

procedure used in all existing EMI elimination methods. Intuitively, this should yield more accurate EMI elimination against the confounding effect of baseline noise in coils. As demonstrated in both simulation and experimental results, Deep-DSP consistently exhibited more effective EMI elimination than EDITER and CNN, especially in presence of strong EMI signals (Figures 2 and 4 vs. Figure S2) or dynamically varying EMI signal relationships between MRI receive coil and EMI sensing coils (Figure S9), and/or with few EMI sensing coils (Figures 5 and 6). Note that the effectiveness and robustness of Deep-DSP could be compromised when using a small number of EMI sensing coils (such as using only one EMI sensing coil; see Figures 5 and 6) and/or insufficient training data (Figure S1).

Deep-DSP uses a residual U-Net model architecture. As illustrated in our recent work,[19,34] a five-layer CNN-based method could yield more effective EMI elimination than analytical transfer function and EDITER methods. This was because the versatile CNN model combines multiple layers of simple functions, with which the EMI signal relationship among coils could be better characterized under realistic and diverse conditions when compared with analytical methods that are based on the simple transfer function concept. Intuitively, a deeper CNN model that leverages prior knowledge about MR

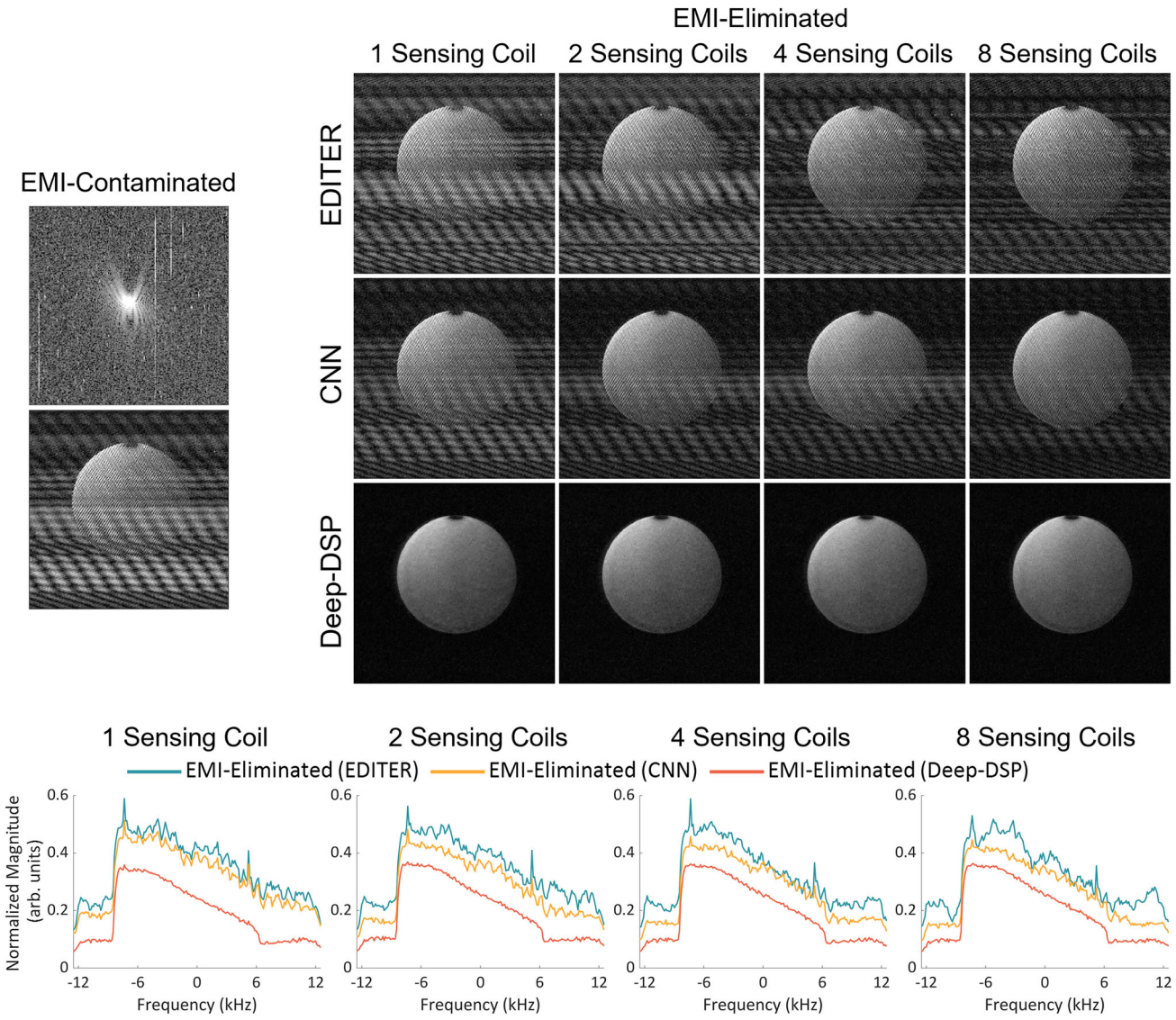

FIGURE 8 Electromagnetic interference (EMI) elimination for 1.5T phantom imaging with incomplete RF shielding (i.e., RF shielding room door open). The phantom data set was acquired on a clinical 1.5T superconducting magnet whole-body MRI scanner, with 63.9-MHz resonance frequency. A head coil with eight channels was used as the MRI receive coils, whereas a separate knee coil with eight channels placed on the patient bed was used as the EMI sensing coils. The outer 50% k-space data acquired by MRI receive coil and EMI sensing coils within the MR signal-acquisition window were treated as EMI characterization data for numerical fitting by EDITER or model training by convolutional neural network (CNN) or deep learning convolutional neural network (Deep-DSP). Images from one channel within the head coil with and without EMI elimination are shown. Deep-DSP was observed to work well at 1.5 T, consistent with 0.055T results.

signal characteristics should also yield improved EMI elimination, especially when EMI characteristics or/and environments become complex. However, training a deep CNN model may be difficult, particularly when the training data size is limited[41] and lacks efficiency. With this practical consideration, this study takes advantages of both U-Net[36] and ResNet[37] by using a residual U-Net model for direct MR signal prediction.

In this study, the model was demonstrated by training using scan-specific data acquired within the EMI signal characterization window during the deadtime of each TR (Figure 1B). The inclusion of such EMI signal characterization window may compromise imaging flexibility when the shortest possible TR is desired, such as in the case of short TR TrueFISP or balanced SSFP imaging. Nevertheless, this study also demonstrated the model training using outer parts of the k-space data acquired within the MR signal acquisition window (i.e., without the need for any separate or dedicated EMI signal characterization). Such trained model produced EMI elimination results largely comparable to those using dedicated EMI characterization data (Figures 3 and 6). Note that previous methods also used data acquired before imaging experiments[42] or entire data

acquired within the MR signal acquisition window (i.e., whole k-space data)[31] for EMI characterization. Their performances could degrade when actual transfer functions alter between EMI characterization data acquisition and MRI data acquisition in the former case, or when MR signal magnitude in k-space is strong in the latter case (as illustrated in our recent study[34]). We recommend the use of dedicated EMI characterization data (Figure 1B) for more accurate EMI characterization and elimination, especially in some scenarios in which 1D temporal FE lines that contain little MR signals are insufficient or not available for Deep-DSP model training (e.g., when the matrix size is small or in 2D radial or spiral imaging). Note that, in reality, the EMI characterization data-acquisition scheme imposes little time-overhead constraints on most clinical MRI imaging protocols.

When preparing training data for Deep-DSP model, EMI-free MR k-space signals from an arbitrarily chosen EMI-free data set are added into experimental EMI-only MRI receive coil signals sampled within the EMI signal-characterization window to synthesize EMI-contaminated MRI receive coil signals. Both simulation and experimental results demonstrated that the trained models were not sensitive to actual image content or contrast of the arbitrary EMI-free data set. As shown in Figures S5–S7 and Figure 7, the model trained using axial T_{2W} brain MR signals accurately predicted T_{1W} brain MR signals and phantom MR signals, as well as coronal T_{1W}/T_{2W}/FLAIR brain MR signals. Thus, Deep-DSP training data preparation incurs no extra requirement or data acquisition in practice. For example, any publicly available EMI-free k-space MRI data set can be used for synthesizing training data for this purpose.

It is noteworthy that Deep-DSP also worked effectively not only for the low-frequency regime (~2.3 MHz) on a 0.055T brain MRI scanner but also for high-frequency regime (~63.9 MHz) on a 1.5T whole-body scanner (Figure 8). These preliminary results, together with our previous 1.5T results,[34,35] demonstrate the potential applicability of the Deep-DSP framework to both ULF and high-field MRI.

The superior EMI elimination performance of the proposed method did not rely on a large training data set (Figure S1). More importantly, the model training converged fast and was computationally efficient. For the simulated brain data set with about 12-k training samples (where EMI signals were acquired with acquisition matrix = 128 × 126 × 32 and NEX = 4), model training took 6 min compared with 1 min for EDITER with a 7 × 7 kernel size and 5 min for our recent CNN method, respectively, on a modest set of Quadro RTX 8000 GPU and Intel Core i9-10 900X CPU. The model architecture is relatively simple, and its parameters can be further optimized in the future to accelerate the training or achieve near real-time EMI elimination.

5 | CONCLUSION

This study develops a new strategy of active EMI sensing and deep learning direct EMI-free MR signal prediction for truly RF shielding-free MRI in pursuit of low-cost, portable, or/and patient-friendly applications. The proposed Deep-DSP not only exploits the coupling relationship between MRI receive coil and EMI sensing coils but also leverages prior knowledge about MR signal characteristics in a data-driven manner. Despite its deep learning nature, Deep-DSP framework is computationally simple and efficient. It yields effective and robust EMI elimination, consistently and significantly outperforming existing methods in terms of substantially improved EMI elimination and use of few EMI sensing coils. Furthermore, it works well without dedicated EMI characterization data. The proposed strategy may also offer a new EMI elimination approach for other RF signal detection applications in the presence of strong and complex EMI emissions beyond MRI.

ACKNOWLEDGMENTS

This study is supported in part by the Hong Kong Research Grant Council (R7003-19F, HKU17112120, HKU17127121, HKU17127022, and HKU17127523 to E.X.W., and HKU17104020, HKU17127021, and HKU17127723 to A.T.L.L.), and the Lam Woo Foundation to E.X.W. The authors thank Drs. Y. Liu, V. Lau, R. Zhu, W Chew, A. Leong, and J. Zhu for their inspiring discussions and technical assistance.

DATA AVAILABILITY STATEMENT

The codes and data that support the findings of this study are available for download from a public repository (https://github.com/bispmri/Deep-DSP) or from the corresponding author upon reasonable request.

ORCID

Yujiao Zhao https://orcid.org/0000-0001-8063-887X
Linfang Xiao https://orcid.org/0000-0002-3508-7842
Jiahao Hu https://orcid.org/0000-0002-3442-9150
Ed X. Wu https://orcid.org/0000-0001-5581-1546

REFERENCES

1. Lauterbur PC. Image formation by induced local interactions: examples employing nuclear magnetic resonance. *Nature.* 1973;242:190-191.
2. Fuchs VR, Sox HC Jr. Physicians' views of the relative importance of thirty medical innovations. *Health Aff.* 2001;20:30-42.

3. Reimer P, Parizel PM, Meaney JFM, Stichnoth FA. *Clinical MR Imaging: a Practical Approach*. Springer; 2010.
4. OECD. Magnetic resonance imaging (MRI) units (indicator). 2021. doi: 10.1787/1a72e7d1-en
5. Cho A. MRI for all. *Science.* 2023;379:748-751.
6. Webb A, Obungoloch J. Five steps to make MRI scanners more affordable to the world. *Nature.* 2023;615:391-393.
7. Naddaf M. One MRI for 4.7 million people: the battle to treat Syria's earthquake survivors. *Nature*. 2023;615:193-194.
8. Geethanath S, Vaughan JT. Accessible magnetic resonance imaging: a review. *J Magn Reson Imaging.* 2019;49:e65-e77.
9. Marques JP, Simonis FFJ, Webb AG. Low-field MRI: an MR physics perspective. *J Magn Reson Imaging.* 2019;49: 1528-1542.
10. Wald LL, McDaniel PC, Witzel T, Stockmann JP, Cooley CZ. Low-cost and portable MRI. *J Magn Reson Imaging.* 2020;52:686-696.
11. Arnold TC, Freeman CW, Litt B, Stein JM. Low-field MRI: clinical promise and challenges. *J Magn Reson Imaging.* 2023;57:25-44.
12. Kimberly WT, Sorby-Adams AJ, Webb AG, et al. Brain imaging with portable low-field MRI. *Nat Rev Bioeng.* 2023;1:617-630.
13. Hennig J. An evolution of low-field strength MRI. *Magma.* 2023;36:335-346.
14. Salameh N, Lurie DJ, Ipek Ö, Cooley CZ, Campbell-Washburn AE. Exploring the foothills: benefits below 1 Tesla? *Magma*. 2023;36:329-333.
15. McDaniel PC, Cooley CZ, Stockmann JP, Wald LL. The MR cap: a single-sided MRI system designed for potential point-of-care limited field-of-view brain imaging. *Magn Reson Med.* 2019;82:1946-1960.
16. Cooley CZ, McDaniel PC, Stockmann JP, et al. A portable scanner for magnetic resonance imaging of the brain. *Nat Biomed Eng.* 2021;5:229-239.
17. O'Reilly T, Teeuwisse WM, de Gans D, Koolstra K, Webb AG. In vivo 3D brain and extremity MRI at 50 mT using a permanent magnet Halbach array. *Magn Reson Med.* 2021;85:495-505.
18. He Y, He W, Tan L, et al. Use of 2.1 MHz MRI scanner for brain imaging and its preliminary results in stroke. *J Magn Reson.* 2020;319:106829.
19. Liu Y, Leong ATL, Zhao Y, et al. A low-cost and shielding-free ultra-low-field brain MRI scanner. *Nat Commun.* 2021;12:1-14.
20. de Leeuw den Bouter ML, Ippolito G, O'Reilly TPA, Remis RF, Van Gijzen MB, Webb AG. Deep learning-based single image super-resolution for low-field MR brain images. *Sci Rep.* 2022;12:6362.
21. Iglesias JE, Schleicher R, Laguna S, et al. Quantitative brain morphometry of portable low-field-strength MRI using super-resolution machine learning. *Radiology.* 2023;306:e220522.
22. Lau V, Xiao L, Zhao Y, et al. Pushing the limits of low-cost ultralow-field MRI by dual-acquisition deep learning 3D super-resolution. *Magn Reson Med.* 2023;90:400-416.
23. Man C, Su S, Lau V, et al. Deep learning enabled fast 3D brain MRI at 0.055 tesla. *Sci Adv.* 2023;9:eadi9327.
24. Mazurek MH, Cahn BA, Yuen MM, et al. Portable, bedside, low-field magnetic resonance imaging for evaluation of intracerebral hemorrhage. *Nat Commun.* 2021;12:5119.
25. Mazurek MH, Yuen MM, Cahn BA, et al. Low-field, portable magnetic resonance imaging at the bedside to assess brain injury in patients with severe COVID-19 (1349). *Neurology*. 2021;96:1349.
26. Sheth KN, Mazurek MH, Yuen MM, et al. Assessment of brain injury using portable, low-field magnetic resonance imaging at the bedside of critically ill patients. *JAMA Neurol.* 2021; 78:41-47.
27. Yuen MM, Prabhat AM, Mazurek MH, et al. Portable, low-field magnetic resonance imaging enables highly accessible and dynamic bedside evaluation of ischemic stroke. *Sci Adv.* 2022;8:eabm3952.
28. Rearick T, Charvat GL, Rosen MS, Rothberg JM. Noise suppression methods and apparatus patent. US Patent No. 9,797,971. 2017.
29. Srivinas SA, Cooley CZ, Stockmann JP, McDaniel PC, Wald LL. Retrospective electromagnetic interference mitigation in a portable low field MRI system. *Proceedings of the 28th Annual Meeting of ISMRM*. ISMRM; 2020:1269.
30. Dyvorne H, Rearick T, Poole M, et al. Freeing MRI from its Faraday cage with interference rejection. *Proceedings of the 29th Annual Meeting of ISMRM*. ISMRM; 2021:749.
31. Srinivas SA, Cauley SF, Stockmann JP, et al. External dynamic Interference estimation and removal (EDITER) for low field MRI. *Magn Reson Med.* 2022;87:614-628.
32. Yang L, He W, He Y, Wu J, Shen S, Xu Z. Active EMI suppression system for a 50 mT unshielded portable MRI scanner. *IEEE Trans Biomed Eng.* 2022;69:3415-3426.
33. Parsa J, O'Reilly T, Webb A. A single-coil-based method for electromagnetic interference reduction in point-of-care low field MRI systems. *J Magn Reson.* 2023;346:107355.
34. Zhao Y, Xiao L, Liu Y, Leong ATL, Wu EX. Electromagnetic interference (EMI) elimination via active sensing and deep learning prediction for RF shielding-free MRI. *NMR Biomed.* 2023;e4956.
35. Zhao Y, Xiao L, Liu Y, Leong ATL, Wu EX. Deep learning driven EMI prediction and elimination for RF shielding-free MRI at 0.055T and 1.5T. *Proceedings of the 30th Annual Meeting of ISMRM*. ISMRM; 2022:3864.
36. Ronneberger O, Fischer P, Brox T. U-net: convolutional networks for biomedical image segmentation. *Proceedings of the Medical Image Computing and Computer-Assisted Intervention–MICCAI: 18th International Conference*. Springer; 2015: 234-241.
37. He K, Zhang X, Ren S, Sun J. Deep residual learning for image recognition. *Proceedings of the IEEE Conference on Computer Vision and Pattern Recognition*. IEEE; 2016:770-778.
38. Zhang K, Li Y, Zuo W, Zhang L, Van Gool L, Timofte R. Plug-and-play image restoration with deep denoiser prior. *IEEE Trans Pattern Anal Mach Intell.* 2021;44:6360-6376.
39. Kingma DP, Ba J. Adam: a method for stochastic optimization. *International Conference on Learning Representations.* ICLR; 2015.
40. Zanche N. RF receivers: signal detection chain, digitization, system noise figures—from MRI signal to bits. *Proceedings of the 25th Annual Meeting of ISMRM*. ISMRM; 2017: 7082.
41. Long J, Shelhamer E, Darrell T. Fully convolutional networks for semantic segmentation. *Proceedings of the IEEE Conference on Computer Vision and Pattern Recognition*. IEEE; 2015:3431-3440.
42. Su J, Pellicer-Guridi R, Edwards T, et al. A CNN based software gradiometer for electromagnetic background noise reduction

in low field MRI applications. *IEEE Trans Med Imaging.* 2022;41:1007-1016.

SUPPORTING INFORMATION

Additional supporting information may be found in the online version of the article at the publisher's website.

Figure S1. Electromagnetic interference (EMI) elimination using EDITER, convolutional neural network (CNN), and the proposed deep learning direct MR signal prediction (Deep-DSP) methods with different sizes of EMI characterization data (data sizes = 12 k, 8 k, 4 k, and 2 k) for simulated brain data set in Figure 2. The EMI elimination results using Deep-DSP yielded smaller normalized RMS errors (NRMSEs) than those using EDITER and CNN methods in general. The results suggested that the improved performance of the Deep-DSP over EDITER and CNN did not critically rely on a large number of training data.

Figure S2. Deep learning direct MR signal prediction (Deep-DSP) method versus existing EDITER and convolutional neural network (CNN) methods for simulated brain data set in Figure 2 with electromagnetic interference (EMI) signal level reduced by a factor of 2.5 when simulating data sets. When EMI signal level was weak, EDITER and CNN obtained EMI elimination performance comparable to the proposed Deep-DSP.

Figure S3. Residual error histograms computed from the error maps corresponding to electromagnetic interference (EMI) elimination results of simulated T_2-weighted (T_{2W}) brain data sets in Figure 2 (A) and Figure S2 (B).

Figure S4. Spectral analysis of the electromagnetic interference (EMI)–eliminated results shown in Figures 5 and 6. Raw T_2-weighted (T_{2W}) brain data sets were acquired in presence of strong broadband (A) and narrowband (B) EMI. The EMI elimination was performed without using EMI characterization data or with different number of EMI sensing coils ($N_s = 1$, 2, 4, and 10). Magnitude averaged spectra of all frequency-encoding (FE) lines further verified the effective EMI elimination performance of deep learning direct MR signal prediction (Deep-DSP).

Figure S5. The proposed electromagnetic interference (EMI) elimination for simulated T_2-weighted (T_{2W}) brain data set. The T_{1W} brain data set acquired at 3 T was used as ground truth. The same EMI data set used for Figure 2 was retrospectively added into the ground truth to form EMI-contaminated data sets. The model trained for the simulated T_{2W} brain data set in Figure 2 was directly applied to predict T_1-weighted (T_{1W}) brain MR signals. The results demonstrated that the trained model was not image contrast–specific.

Figure S6. The proposed electromagnetic interference (EMI) elimination for simulated phantom data set. The phantom data set acquired at 3 T was used as ground truth. The same EMI data set used for Figure 2 was retrospectively added into the ground truth to form EMI-contaminated data sets. The model trained for the simulated T_2-weighted (T_{2W}) brain data set in Figure 2 was directly applied to predict phantom MR signals. The results demonstrated that the trained model was not image content–specific.

Figure S7. EMI elimination results of experimental shielding-free 0.055T brain data set in Figure 4B using the deep learning direct MR signal prediction (Deep-DSP) model trained with 3T or 0.055T electromagnetic interference (EMI)–free MR signals. The 0.055T EMI-free MR signals for synthesizing EMI-contaminated MRI receive coil signals were obtained by acquiring T_2-weighted (T_{2W}) brain k-space data on the 0.055T brain MRI scanner with RF shielding cage installed and then performing EMI elimination using the convolutional neural network (CNN) method to remove EMI signals generated by internal scanner electronics. The Deep-DSP model trained with 0.055T EMI-free T_{2W} brain signals yielded comparable EMI elimination results as the Deep-DSP model trained with 3T EMI-free T_{2W} brain signals.

Figure S8. The proposed deep learning direct MR signal prediction (Deep-DSP) electromagnetic interference (EMI) elimination for experimental shielding-free 0.055T brain data sets in Figure 4 using 10 EMI sensing coils or no EMI sensing coils. Raw T_2-weighted (T_{2W}) brain data sets were acquired in presence of strong broadband (A) and narrowband (B) EMI. Without any EMI sensing coils, the Deep-DSP model was trained using only synthesized EMI-contaminated MR signals as model inputs, whereas EMI-free MR signals served as model targets. The EMI elimination performance of Deep-DSP was largely degraded as expected. However, it still reduced the EMI artifacts, suggesting that the Deep-DSP method could leverage prior knowledge about MR signal characteristics for EMI elimination.

Figure S9. Electromagnetic interference (EMI) elimination for experimental shielding-free 0.055T brain imaging in presence of subject body position change. Four individual data sets were sequentially acquired from a normal adult using the 4-average 3D fast spin echo (FSE) fluid-attenuated inversion recovery (FLAIR) protocol. A moderate subject position change was caused by bending of lower legs during the third acquisition. This evaluation is relevant to some realistic EMI elimination scenarios, in which dynamically varying EMI signal relationships between MRI receive coil and EMI sensing coils can be caused by subject position changes or movements of nearby attending staff and equipment during scan. The

EMI elimination was performed by EDITER with different thresholds ($\delta = 0.5$, 0.95, 0.97, and 0.99), convolutional neural network (CNN), and the proposed deep learning direct MR signal prediction (Deep-DSP) methods. The brain images without and with EMI removal before averaging are shown on the left, whereas the images averaged from four acquisitions are shown on the right. With smaller or larger threshold, the EDITER EMI elimination was suboptimal, exhibiting pronounced residual EMI artifacts as indicated by arrows. Furthermore, the proposed Deep-DSP method outperformed EDITER with manually optimized threshold.

Table S1. SNR quantification corresponding to electromagnetic interference (EMI) elimination results of simulated T_2-weighted (T_{2W}) brain data sets in Figure 2 (A) and Figure S2 (B).

Table S2. SNR quantification corresponding to electromagnetic interference (EMI) elimination results of experimental shielding-free 0.055T brain data sets in Figure 4. Raw T_2-weighted (T_{2W}) brain data sets were acquired in presence of strong broadband (A) and narrowband (B) EMI.

How to cite this article: Zhao Y, Xiao L, Hu J, Wu EX. Robust EMI elimination for RF shielding-free MRI through deep learning direct MR signal prediction. *Magn Reson Med*. 2024;92:112-127. doi: 10.1002/mrm.30046